


Article

# Novel Energy Management Control Strategy for Improving Efficiency in Hybrid Powertrains

Alberto Broatch , Pablo Olmeda \*, Benjamín Plá and Amin Dreif

CMT-Motores Térmicos, Universitat Politècnica de València, Camino de Vera s/n, 46022 València, Spain

\* Correspondence: pablogon@mot.upv.es; Tel.: +34-963877650

**Abstract:** Energy management in electrified vehicles is critical and directly impacts the global operating efficiency, durability, driveability, and safety of the vehicle powertrain. Given the multitude of components of these powertrains, the complexity of the proper control is significantly higher than the conventional internal combustion engine vehicle (ICEV). Hence, several control algorithms and numerical methods have been developed and implemented in order to optimize the operation of the hybrid powertrain while complying with the required boundary conditions. In this work, a model-based method is used for predicting the impacts of a set of possible control actions, choosing the one minimizing the associated costs. In particular, the energy management technique used in the present study is the equivalent consumption minimization strategy (ECMS). The novelty of this work consists of taking into account the thermal state of the ICE for optimization. This feature was implemented by means of an extensive experimental campaign at different coolant temperatures of the ICE to calibrate the additional fuel consumption due to operating the engine outside of its optimum temperature. The results showed significant gains in both WLTC and RDE cycles.

**Keywords:** 1D modeling; ICE thermal state; optimization; hybrid vehicles; ECMS



**Citation:** Broatch, A.; Olmeda, P.; Plá, B.; Dreif, A. Novel Energy Management Control Strategy for Improving Efficiency in Hybrid Powertrains. *Energies* **2023**, *16*, 107. <https://doi.org/10.3390/en16010107>

Academic Editor: Javier Contreras

Received: 17 November 2022

Revised: 15 December 2022

Accepted: 16 December 2022

Published: 22 December 2022



**Copyright:** © 2022 by the authors. Licensee MDPI, Basel, Switzerland. This article is an open access article distributed under the terms and conditions of the Creative Commons Attribution (CC BY) license (<https://creativecommons.org/licenses/by/4.0/>).

## 1. Introduction

In view of the current sociopolitical restrictions and market demands, the automotive industry has invested a great amount of effort into electrified vehicles [1]. Furthermore, the worldwide electric vehicle (EV) market share is expected to grow 26.8% each year until 2030 while the production and selling of conventional internal combustion engine vehicles (ICEVs) will be strongly reduced [2]. Although the costs of battery electric vehicles (BEVs) have decreased, they are still higher than their competitors (i.e., hybrid electric vehicles (HEVs) and ICE vehicles...). Additionally, the absence of sufficient recharging infrastructure, limited travel ranges, and charge times are still critical drawbacks for full electric vehicles [3].

Hybrid vehicles benefit from the advantages of ICEs (i.e., range, energy, and power density...) and electrification (i.e., lower tailpipe emissions and a reduction of noise...). Hence, they provide optimum solutions for the transition from ICEVs to BEVs [4]. The propulsive system of the hybrid vehicle presents high complexity and requires advanced control of the different subsystems. In fact, the energy management system (EMS) of the HEV is fundamental for efficiently operating the propulsive system while complying with the required power and safety requirements [5]. To achieve this goal, several research studies have been published using different methodologies and requirements [6,7].

On the one hand, dynamic programming (DP) and Pontryagin's minimum principle (PMP) are numerical methods widely used in vehicle optimization [8,9]. The control strategies are not casual and require pre-known velocity profiles of the vehicles. On the other hand, model predictive control (MPC) and an equivalent consumption minimization strategy (ECMS) have been implemented for online optimization [10,11]. In [12], Hwang applied the ECMS to optimize the performance of fuel consumption in an advanced

hybrid system. The results showed benefits of around 8% when compared to a rule-based control strategy. Zhang et al. proposed a short-term optimal control based on MPC that considers the transient motion of the powertrain, significantly improving the engine fuel's consumption [13].

However, few research studies have been published that consider the thermal state of the engine, especially with experimental validation [14]. Chu et al. implemented an energy management strategy, considering the warming up of the engine using the DP algorithm to optimize fuel consumption. Results showed gains of up to 2% [15]. Lescot et al. combined both a thermal management system and an energy management strategy based on ECMS by implementing the engine's thermal state in the cost function [16]. Gains on fuel consumption varied between 2.8% and 0.64%, depending on the transient cycle.

Therefore, model-based methods that can predict the impacts of possible control actions and choose the one minimizing the associated costs, have shown potential in exploiting the advantages of xEVs. The method proposed in this work follows this second path because of two main reasons: (1) it has better potential to optimize energy consumption compared to heuristic methods and (2) it provides the best possible powertrain performance in each scenario. It is a very powerful tool used to compare different design decisions in a fair way since the control strategy will be optimized for each particular design.

In this work, an EMS based on the ECMS was implemented in an integrated virtual power plant for a series-parallel hybrid vehicle architecture. The developed control took into consideration the thermal state of the engine and its impact on the overall efficiency. In order to assess the engine fuel consumption variation with the temperature, an extensive experimental campaign was carried out at different engine coolant temperatures. The validation of the control strategy was carried out in the test bench and further simulations were performed to evaluate fuel gain in real driving emission cycles (RDEs).

## 2. Materials and Methods

### 2.1. Experimental Testing

In this section, a description of the experimental campaign performed with the ICE is presented. This is a 3-cylinder 999 cm<sup>3</sup> spark ignition engine.

The engine features are summarized in Table 1.

**Table 1.** Engine specifications used for validation of the ICE models.

Parameter	Value
Displacement	999 cm <sup>3</sup>
Diameter	81.3 mm
Stroke	72.2 mm
Number of cylinders	3 in line
Number of valves	4 per cylinder
Max torque @ speed	182.3 Nm @ 2250 rpm
Max power @ speed	83.0 kW @ 5250 rpm

The measurements were performed on a highly instrumented test bench. The test bench was equipped with state-of-the-art components that allow the operation of the engine in RDE transient conditions [17]. Several driving cycles, including RDE and the WLTC, were tested in order to assess the impacts of the thermal management on the fuel consumption of a HEV, particularly, to evaluate the improvements achieved with the proposed control strategy. The RDE cycle was carried out in the laboratory with constant temperature and atmospheric pressure. All of the tests and simulations were conducted under those conditions. All of the tests and simulations were conducted at those conditions. Additionally, the experimental campaign performed for this work considered several steady-state running conditions within the engine performance map. The tested conditions were the following:

- Sixty-three points from the low load (3 BMEP) to high load (around 22 BMEP) covering a wide range of the engine map at different engine speeds.
- The measurements were repeated at different coolant temperatures: 35 °C, 50 °C, 63 °C, 76 °C, and 88 °C.

The test bench was equipped with different measurement tools that were thoroughly calibrated before the measurement campaign. Several temperature-, mass flow-, and pressure sensors were installed in the gas circuit and hydraulic circuits of the engine. All were calibrated and connected to a data acquisition system. Table 2 summarizes the main instrumentation equipment.

**Table 2.** Laboratory instrumentation.

Variable	Instrument	Range	Accuracy
Engine speed	Dynamometer	0–7500 rpm	±1 rpm
Torque	Dynamometer	0–400 Nm	±0.5%
Fluid temperature	k-type thermocouple	70–1520 K	±2 K
Air mass flow	Flowmeter	0–1700 kg/h	±2%
In-cylinder pressure	AVL GH13P	0–200 bar	±0.3%
Coolant flow	OPTIFLUX 4000	4.5–90 lpm	±0.5%
Oil pressure	Piezoresistive transducer	0–10 bar	±25 mbar
Emissions	Horiba MEXA @ AVL Smoke meter		

Coolant temperatures were measured at different places of the engine cooling circuit (i.e., before and after the engine, turbocharger, and oil cooler). Coolant flows were measured in three different paths as can be seen in Figure 1. The oil temperature and pressure were also measured in the oil sump and after the oil cooler, respectively.

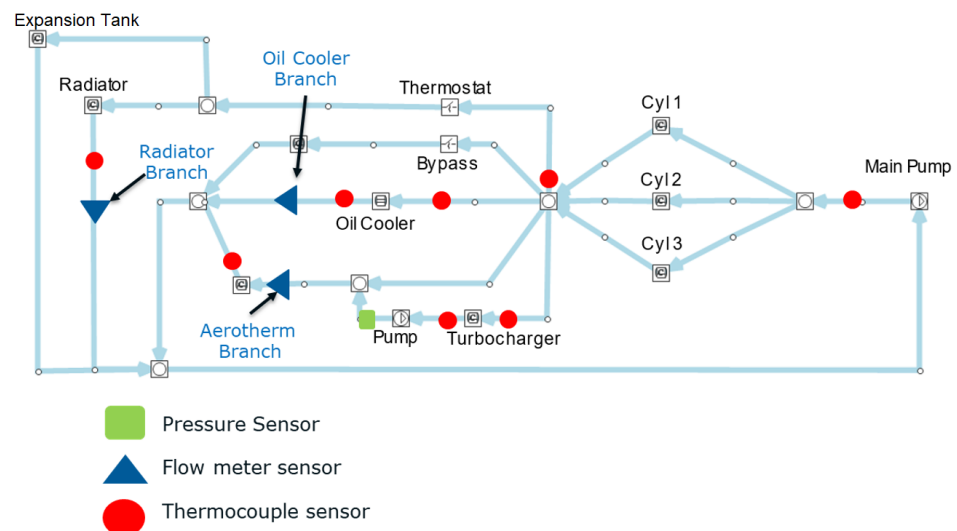


**Figure 1.** ICE coolant circuit layout.

## 2.2. Numerical Model

In order to carry out the study, an integrated virtual model in MATLAB–Simulink was developed, including all subsystems of the hybrid propulsive system (i.e., battery, electric drive, ICE, transmission, vehicle, driver...). Figure 2 shows a schematic view of the hybrid vehicle submodels.

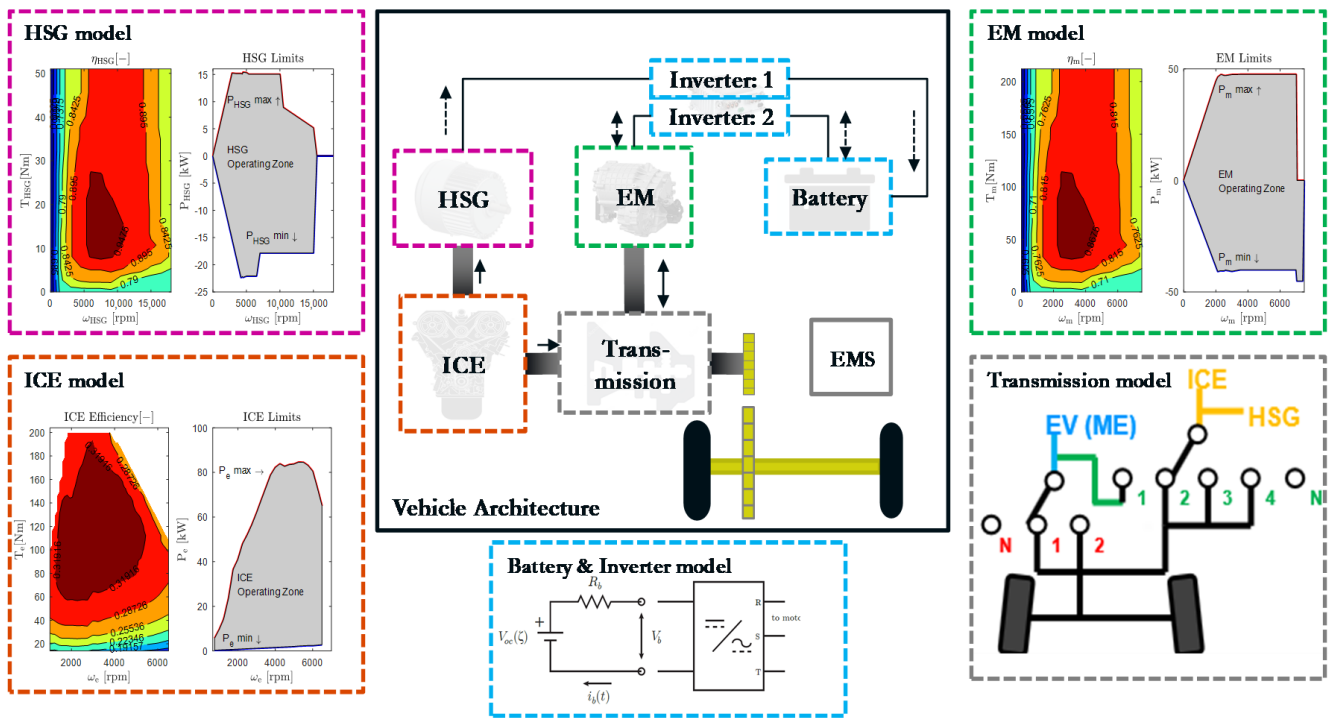


Figure 2. Virtual components of the hybrid vehicle.

2.2.1. Internal Combustion Engine

Two modeling approaches can be used in the model depending on the purpose. The model implemented in the control strategy, i.e., the one used to make decisions on the power split to minimize fuel consumption, is a simple model based on a quasi-steady approach with an engine map and corrections to consider the engine dynamics and impacts of the factors, such as the thermal state. Note that model simplicity is required in the model-based control since several control decisions must be evaluated at every time-step to choose the optimal one. The model in the plant, which is used to check the impact of the control strategy, may be based on the previous steady-state approach or a detailed model (the 1D-model), which can be embedded by means of an S-function or FMU (functional mock-up unit). The present section is focused on the control-oriented model.

The ICE model follows the classic approach for energy management, consisting of reducing the engine model to a map of any interesting variable, depending on the engine speed and throttle. Among the most interesting variables to map, one can find the torque, fuel consumption, efficiency, or emissions. Regarding the accuracy of this method—modeling complex and dynamic variables, such as emissions, is limited; however, this approach can provide fair enough results in terms of fuel consumption, at least to make control decisions. Figure 3 shows an example of this map for BSFC in warm conditions in the engine. The data are obtained by sweeping the range of operating conditions in the test bench.

Since maps such as that of Figure 3 are obtained in steady-state conditions, they cannot capture transient phenomena. One can think of two main transient phenomena affecting ICE. The first one may be a variation of the operating conditions (engine speed and throttle) that will lead to a delayed and filtered response of the torque. The second transient phenomenon strongly affecting the engine performance is the warm-up, since variations in the thermal state of the engine will lead to changes in the heat transfer and friction phenomena, which will finally affect the performance. In this sense, the model employed for control purposes is based on Equations (1) and (2):

$$M_e^0 = f(n_e, \alpha) \tag{1}$$

$$m_e^0 = g(n_e, \alpha) \quad (2)$$

where  $f$  and  $g$  map the engine speed  $n_e$  and throttle to  $\alpha$  the corresponding variable (reference effective torque  $M_e^0$ , reference fuel consumption  $m_e^0$ ) by means of interpolation in a database. In the case at hand,  $f$  and  $g$  are 2D-lookup tables. The term references in previous variables highlight that those variables have been obtained in a steady state (and warm conditions).

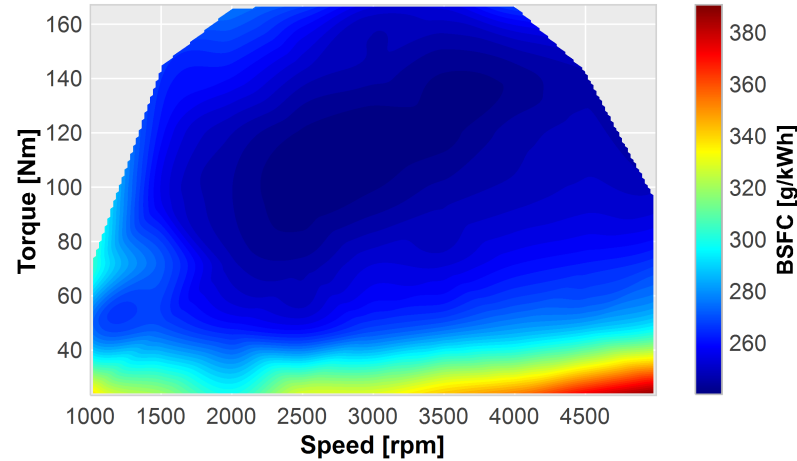


**Figure 3.** ICE fuel consumption 2D map depending on the engine speed and torque.

Regarding the impacts of variations in the engine operations, a filter on the reference torque was applied. The filter has the following Equation (3):

$$M_e^k = aM_e^{k-1} + bM_e^{0,k} \quad (3)$$

where superscript  $k$  stands for the time-step, parameter  $a$  represents the influence of the torque value in the previous time-step in the current one (state matrix), and  $b$  is the weight of the current reference torque in the actual torque (input matrix). Choosing  $0 \leq a \leq 1$  and  $b = 1 - a$  leads to a filter with the gain equal to one whose time constant increases with  $a$  and the steady state  $M_e^k = M_e^{0,k}$ . The values of  $a$  and  $b$  can be obtained by calibration using the engine transient test and minimizing the error between the measured and model torque. Note that the values of  $a$  and  $b$  will depend on the time step of the simulation. Regarding the impact of the engine's thermal state on fuel consumption, a lumped heat transfer model was used. In this sense, the thermal state of the engine was approximated by a global temperature (assumed to be that of the coolant  $\theta_c$ ) as Equation (4) shows:

$$\dot{\theta}_c^k = \frac{1}{C_c} \left( hA(\theta_c^k - \theta_{env}) + k(1 - \eta_e) \dot{m}_f^k H_c \right) = k_{0c} + k_{1c}(\theta_c^k - \theta_{env}) + k_{2c}(P_f^k - P_e^k) \quad (4)$$

where  $k_{0c}$  and  $k_{1c}$  model the heat transfer between the engine and the environment (so their values depend on the cooling circuit conditions) and  $k_{2c}$  represents the contribution of the energy released in the fuel combustion, which is not transformed in the mechanical power. Constants  $k_{0c}$ ,  $k_{1c}$ , and  $k_{2c}$  will, in general, depend on the operating conditions. In the case at hand, they have different values if the engine is on or off, and the temperature is saturated to 100 °C, assuming that the coolant circuit is able to avoid any coolant temperature excursion above that value ( $\theta_c^k \leq 100$  °C).

Once the thermal state is determined by Equation (4), the reference fuel consumption can be corrected with Equation (5):

$$m_f = m_f^0 h(n, \alpha, \theta_c) \quad (5)$$

where  $h(n, \alpha, \theta_c)$  is the experimentally calculated ratio (rearranging Equation (5)) between experimental measurements at different coolant temperatures for each engine operating point. Several steady-state operating conditions were measured at different coolant temperatures (35 °C, 50 °C, 63 °C, 76 °C, and 88 °C). Using these data, the  $\frac{\partial h(n, \alpha, \theta_c)}{\partial \theta_c}$  3D map was generated and implemented in the control model. As can be observed in Figure 4, the measurements show that operating the engine at a higher temperature has a great impact on fuel savings. For example, operating the ICE at 35 °C could mean a 20% increase in the fuel consumption. Two main reasons explain this fuel consumption increase. On the one hand, lower coolant temperatures of the engine directly mean lower oil temperatures (both the coolant and oil hydraulic circuits are connected by the oil cooler), which increases the friction losses due to higher oil viscosity. On the other hand, lower temperatures in the cylinder block and head increase the temperature drop between the material and the gas, hence, increasing heat transfer and decreasing the combustion efficiency (engine minus the adiabatic).

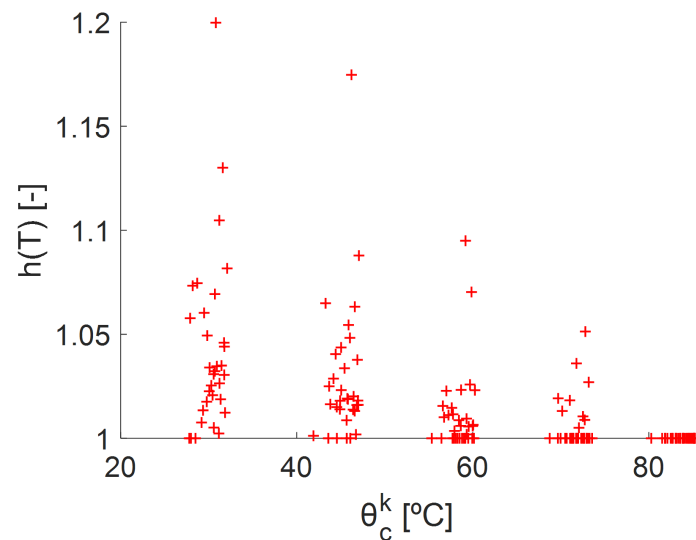


**Figure 4.**  $h(n, \alpha, \theta_c)$  3D Map of fuel consumption ratio with the engine coolant temperature.

Figure 5 shows the evolution of the coolant temperature in a RDE with the ICE. Results show how despite a simple model, it is able to capture (to some extent) the evolution of the coolant temperature in a dynamic cycle, such as a RDE.

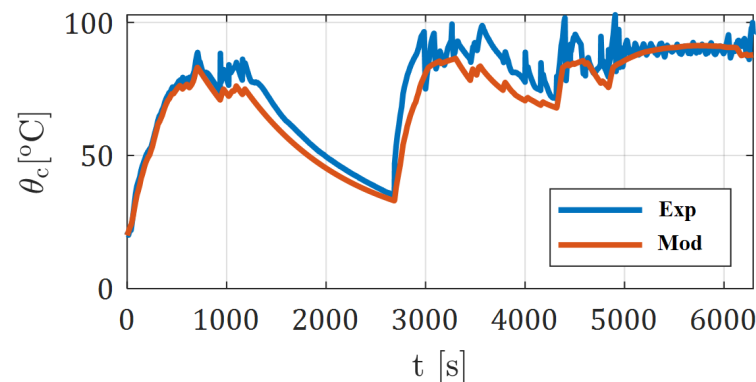


**Figure 5.** Evolution of the coolant temperature in a RDE with the ICE. Comparison between experimental results and control-oriented model.

### 2.2.2. Electric Machine and Power Electronics

The control-oriented model employed in this work considers quasi-steady behavior, i.e., the dynamics of the processes inside the electric motor are much faster than the characteristic times of the driving cycles and the consequent evolution of the main vehicle variables. This hypothesis becomes valid since, in general, the motor response is much faster than the ICE dynamics and strongly simplifies the model since the typical motor map—as supplied by a manufacturer representing the efficiency as a function of the motor speed and torque—can be directly applied. The model assumes that the motor can instantaneously supply the demanded torque if it does not exceed the maximum allowed value that may depend on the motor speed. In this sense, the torque in the motor shaft is calculated according to Equation (6):

$$T_m = \min(T_m^{max}(\omega_m), \max(-T_m^{max}(\omega_m), T_m^{dem})) \quad (6)$$

where  $T_m^{dem}$  is the torque demand and  $T_m^{max}(\omega_m)$  is the maximum torque that the motor is able to produce or absorb at a certain speed  $\omega_m$ . Taking into account the efficiency map of the electric machine ( $\eta_m$ ), Equations (7)–(9) were used to calculate the electric power consumption of the motor  $P_m^{elec}$ :

$$\eta_m = f(\omega_m, u_{Tm}) \quad (7)$$

$$u_{Tm} = \frac{T_m}{T_m^{max}(\omega_m)} \quad (8)$$

$$P_m^{elec} = \begin{cases} T_m \omega_m \eta_m & \text{if } \omega_m T_m \leq 0 \\ \frac{T_m \omega_m}{\eta_m} & \text{if } \omega_m T_m > 0 \end{cases} \quad (9)$$

where cases with the motor braking or propelling are distinguished. Note the non-causality of the model since in the actual system, the torque at the motor shaft is a consequence of the supplied electrical power at a particular rotational speed, and the model follows the inverse path (computes the electrical power consumption from the torque and speed). In this sense, the model assumes that all of the torque demanded by the motor is instantaneously supplied (except when the maximum or minimum torques are exceeded). All of the electric machines (motors and generators) are modeled in the same way and the power electronics are modeled as efficiencies, which are included in the map of Equation (7).

### 2.2.3. Battery

The control-oriented model of the battery used in this work is a Thevenin equivalent circuit consisting of an ideal voltage source and a resistor in the series, as displayed in Figure 6.

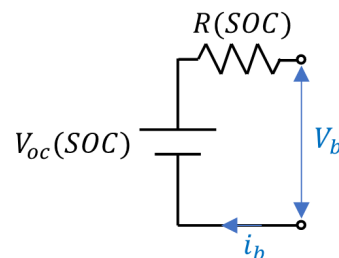


**Figure 6.** Scheme of the battery model using its Thevenin equivalent circuit.

According to the previous circuit, the battery voltages at the terminals follow Equation (10):

$$V_b = V_{oc} - Ri_b \quad (10)$$

where  $i_b$  represents the current drawn from the battery and the open-circuit voltage ( $V_{oc}$ ), and the internal resistance ( $R$ ) is the model parameter used to experimentally identify, which may depend on the state of charge of the battery (SOC). Despite the parameter's identification being outside the scope of the work, the interested reader is referred to [18] for a detailed explanation of the methods used for parameter identification. The rate of change in the battery charge ( $Q_b$ ) is the current (Equation (11)).

$$\dot{Q}_b = -\eta_b i_b \quad (11)$$

where the term  $\eta_b$  represents a coulombic efficiency, lessening the variation of the battery charge during recharging. From the previous expression, one can compute the battery charge in each time ( $t$ ), which can be computed by the current integration according to Equation (12):

$$Q_b(t) = Q_b(t_0) - \int_{t_0}^t \eta_b i_b(\tau) d\tau \quad (12)$$

The state of charge of the battery is the variable governing the Thevenin equivalent circuit parameter, and represents the ratio between the battery charge and its maximum value, as seen in Equation (13).

$$SOC(t) = \frac{Q_b(t)}{Q_b} \quad (13)$$

Provided that the model input is the power demanded by the motor and the output is the SOC, the circuit in Figure 6 is solved for the current variable following Equation (14):

$$i_b = \frac{V_{oc} - \sqrt{V_{oc}^2 - 4RP_{motor}^{elec}}}{2R} \quad (14)$$

where the power demand of the motor should be replaced by the total power demand of the electric machines if more than one is used (e.g., series HEV).

#### 2.2.4. Transmission

The energy transmission from the engine and motor output to the wheel is done by several clutches and gearing systems whose type and arrangement strongly depend on the powertrain type. In this sense, providing a general model is challenging. The powertrain has some degree of generality since it can operate in series and parallel, so the control-oriented model developed in this activity contains both operation modes. Figure 7 shows the architecture where the vehicle can operate in a pure electric mode by selecting gears 1 or 2 in the motor (M) side and neutral on the engine (ICE) side. It can operate in parallel mode by independently choosing the gears of the motor and engine branches. The system can also operate as an ICE-propelled powertrain by selecting 'neutral' for the motor and any of the four available gears for the engine. Finally, the system can operate as a series powertrain where the motor is connected to the wheels through gears 1 or 2 and the engine is connected to the generator (G) through gear S to produce electricity.

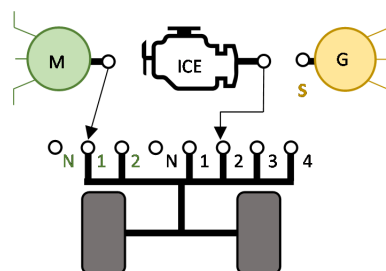


Figure 7. Powertrain architecture of the vehicle, including the parallel and series operation.



The transmission is modeled as a discrete set of gear ratios with fixed efficiency, so the kinematics and energy balance allow computing the speed of the element upstream the transmission, the torque transferred to the transmission output axis from the speed downstream the transmission, and the torque applied to the input axis according to Equations (15) and (16):

$$\omega_{us} = \omega_{ds} R_g \quad (15)$$

$$M_{ds} = M_{us} R_g \eta_g \quad (16)$$

where  $R_g$  and  $\eta_g$  are the transmission ratio and efficiency, which depend on the selected gear.

### 2.2.5. Vehicle Dynamics

The model is based on longitudinal vehicle dynamics and solves the Newton equation at every time step to obtain the vehicle acceleration from the balance between the traction and resistive forces (or torques). In this sense, the main terms participating in the energy balance are:

- A source term representing the net torque coming from the powertrain, including the power split, efficiency, and gear transmission ratio. Additionally, the braking torque may be applied if the driver acts on the brake pedal to reduce the vehicle speed and the motor is not able to absorb the braking power.
- An inertial term, including the vehicle mass and powertrain inertia.
- A set of sink terms considering non-conservative forces, mainly friction losses due to aerodynamic drag and rolling resistance.
- An additional term may be included to consider the potential energy, allowing the assessment of the road slope effects (despite tests carried out in the present project have been conducted, considering a horizontal road).

The previous terms can be combined in Newton's law (in the torque formulation) according to Equation (17):

$$M_{wheel} = m_{Veh} \dot{v} r_{wheel} + J_{pwt} \dot{\omega}_{wheel} + m_{Veh} g \sin(\beta) r_{wheel} + \mu m_{Veh} g \cos(\beta) r_{wheel} + \frac{1}{2} \rho S C_x v^2 r_{wheel} \quad (17)$$

where the variables are defined in Table 3.

**Table 3.** Variable definitions of Equation (17).

Variable	Definition
$M_{wheel}$	Net torque applied at the wheels
$m_{Veh}$	Vehicle mass
$J_{pwt}$	Global powertrain inertia
$r_{wheel}$	Wheel effective radius
$v$	Vehicle linear speed
$\dot{v}$	Vehicle linear acceleration
$\dot{\omega}_{wheel}$	Wheel angular acceleration
$g$	Gravity acceleration
$\beta$	Track slope
$\mu$	Dynamic coefficient of rolling friction
$\rho$	Environment air density
$S$	Vehicle frontal area
$C_x$	Longitudinal aero drag coefficient

Hence, if the total torque applied to the wheel is known (from the application of the engine, motor, and transmission models), Equation (17) can be solved for the acceleration and the vehicle speed can be calculated by the integration. Therefore, the presented vehicle model can work as a closed-loop system, where the torque is progressively transmitted from the engine and motor to the wheels and then is used to obtain the vehicle speed. Moreover, this vehicle speed is necessary to know the engine and motor operating points in

the next step. There is a bidirectional information flow: the torque ( $M$ ) goes from the engine and motor blocks to the vehicle dynamic block, while speed ( $v$ ) goes from the vehicle dynamic block to the engine and motor blocks.

Despite the simplicity of Equation (17), some of the coefficients (e.g., the  $J_{pwt}$  in the case of a complex powertrain, such as a HEV) are difficult to find; for this reason, the following expression (Equation (18)) is used instead:

$$\dot{v} = \frac{M_{wheel}r_{wheel} - (A + Bv + Cv^2)}{m_{eq}} \quad (18)$$

where parameters  $A$ ,  $B$ ,  $C$ , and  $m_{eq}$  are experimentally characterized in a coastdown test.

### 2.2.6. Driver

The objective of the driver model is to follow a given vehicle speed profile as accurately as possible. In this sense, the driver model takes a predefined sequence of vehicle speeds and modifies vehicle actuators (throttle and brake, the gear is automatically selected according to the efficiency criteria by the control strategy) to follow the desired set points. In this sense, the driver model implemented is a proportional–integral (PI) controller acting on a torque demand to cancel the error between the current vehicle speed and a reference.

### 2.3. Control Strategy

The energy management technique used in the present work was the equivalent consumption minimization strategy (ECMS), which consists of a greedy algorithm based on Pontryagin's minimum principle (PMP). Provided there is a power demand, a set of candidates are defined (combinations between the different energy sources) to provide this target, and then the option that minimizes a defined cost function in this time-step is chosen. The cost function is a weighted average of the power delivered by the different energy sources (e.g., fuel from a tank and electricity from a battery), while other criteria or constraints can be added to the cost function with the corresponding weighting factor. In this sense, the weighting factors played key roles in the optimization and were properly calibrated. The next sections provide descriptions of the basics of the ECMS and its application in the present work.

Pontryagin's minimum principle states the necessary conditions for the minimization of a dynamic problem; Equation (19) shows:

$$\arg \min_u J(x, u, w, t) \quad (19)$$

subject to:  $\dot{x} = f(x, u, w, t)$  and  $J = \int_{t_0}^{t_f} L(x, u, w, t)dt + \psi(x(t_f))$ .

Where  $J$  is a cost function and  $f$  is a generic state function describing the evolution of the system states ( $x$ ) with respect to the time ( $t$ ) when a series of control actions ( $u$ ) and disturbances ( $w$ ) are applied. The cost function consists of an integral term defined in  $L$  and a terminal cost ( $\psi(x(t_f))$ ), which may penalize deviations from a final desired state. One can see that the energy management problem perfectly fits in the framework described by Equation (19), a transcription can be found in Table 4.

Considering the Hamiltonian function ( $H$ ), whose definition is presented in Equation (20):

$$H(x, u, w, t) = L(x, u, w, t) + \lambda^T(t)f(x, u, w, t) \quad (20)$$

where the co-state vector  $\lambda$  (with as many elements as states in the problem) is a time varying Lagrangian multiplier aimed to adjoin the system dynamics  $f$  to the cost function. As previously stated, PMP provides the conditions that an optimal solution ( $u^*$ ) to the problem in Equation (18) should fulfill:

1. The optimal solution to the problem described in Equation (19) should minimize the Hamiltonian (Equation 20) in every time step according to Equation (21):

$$u^*(t) = \arg \min_u H(x, u, \lambda, w, t) \quad (21)$$

2. The optimal solution to the problem described in Equation (19) should lead to Equation (22):

$$H(t_f) = -\psi(x(t_f)) \quad (22)$$

3. The evolution of the co-state for the optimal solution should fulfill Equation (23):

$$\dot{\lambda}(t) = -\frac{\partial H}{\partial x} = -\frac{\partial L}{\partial x} - \lambda \frac{\partial f}{\partial x} \quad (23)$$

4. The terminal co-state should be Equation (24):

$$\lambda(t_f) = \frac{\partial \psi(t_f)}{\partial x} \quad (24)$$

**Table 4.** Transcription of the energy management problem to the mathematical framework of the optimal control.

Symbol	Description	Variable in the Energy Management Strategy
$u$	Control action vector	Power split
$x$	State vector	State of Charge of the Battery (SOC), engine thermal state (coolant temperature)
$w$	Disturbance vector	Vehicle speed profile, route height profile, wind velocity and direction
$L$	Lagrangian cost	Fuel consumption, energy consumption, weighted average between energy consumption and pollutants
$\psi$	Terminal cost	Deviation of a target SOC, emissions exceeding certain limit

For the case of energy management, Equations (21) and (23) allow calculating the solution to the problem if a solution exists and is unique. In particular, the algorithm used in this project is based on a shooting method with the following steps:

1. Assign the initial values of the states to the optimal state trajectory ( $x^*(t_0) = x_0$ ).
2. Estimate an initial value for the co-state vector ( $\lambda^*(t_0) = \lambda_0$ ).
3. Compute the optimal control action ( $u^*$ ) at the current time-step by applying Equation (21) by trying a set of candidates.
4. Compute the state derivative  $f(x, u^*, \lambda, w, t)$  and integrate to obtain state  $x$  in the next time-step.
5. Compute the co-state derivative by Equation (23) and integrate to obtain the co-state vector  $\lambda$  in the next time-step.
6. Repeat steps 3–5 until the end of the problem.
7. If the target state at the end of the problem is achieved ( $x(t_f) = x_{t_f}$ ),  $\lambda_0$  is a good guess, otherwise modify  $\lambda_0$  and repeat steps 3–6.

Figure 8 shows a scheme of the solution algorithm explained in points 1–7.

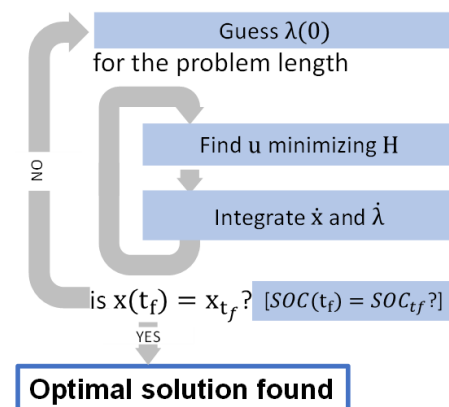


Figure 8. PMP solution algorithm.

An important issue for numerically solving the PMP is that the ordinary differential equations for the co-state integration are generally ill-conditioned and lead  $\lambda$  to blows, even with tight tolerances. In the HEV cases, the following simplification is usually considered to avoid co-state integration. Consider that the Lagrangian cost is the fuel consumption ( $L = m_f$ ) and the state of the problem is the battery state of charge ( $x = SOC$ ). Then, from Equation (23), Equation (25) is obtained:

$$\dot{\lambda}(t) = -\frac{\partial H}{\partial x} = -\frac{\partial m_f}{\partial SOC} - \lambda \frac{\partial f}{\partial SOC} \quad (25)$$

where the first term on the right side is clearly 0, since the fuel consumption depends on the engine speed and throttle (that also depend on the power split) but does not depend explicitly on the SOC. The second term represents how the battery behavior depends on the SOC, so if the battery parameters ( $R, V_{oc}$ ) do not depend on the SOC, the second term will also be 0,  $\lambda$  will be constant, and the co-state integration can be avoided. This simplification is usually considered since it strongly simplifies the online implementation. Note that, provided a constant  $\lambda$ , the Hamiltonian can be interpreted as an equivalent fuel consumption that includes both the fuel and the weighted battery power. This is the basis of ECMS, which, provided an equivalence factor ( $s$ ), chooses the control candidate that minimizes at every time step a weighted average of the fuel consumption and battery power ( $m_f + sPb$ ) according to Equation (26):

$$u^*(t) = \arg \min_u m_f + sPb \quad (26)$$

Note the similarity between Equations (21) and (26). In the same way with PMP, a shooting method is required to find the proper value of  $s$ . As  $s$  approaches 0, the use of the battery becomes cheaper, which leads to lower fuel consumption and battery depletion; on the contrary, an excessively high value of  $s$  will lead to battery overloading and high fuel consumption. A target SOC at the end of the cycle (usually equal to the initial values in HEVs and the minimum allowed SOC in the case of PHEVs) provides the closing condition for the shooting method. As the proper value of  $s$  depends on the driving cycle, the shooting method requires several runs of the driving cycle to find the proper value, which is only possible for offline optimization. For online implementation, since the optimal value of  $s$  is unknown a priori, its value would be online-adapted according to the differences between the measured and the target SOC, usually with a PID.

### 2.3.1. Modifications to Deal with Oscillating Behavior

In order to make the proposed control strategy more robust, general, and able to deal with xEVs having different possible modes (e.g., series, parallel), considering other system states (i.e., the engine coolant temperature), some modifications were introduced.

Under certain circumstances, the direct application of Equation (26) can produce policies resulting in poor drivability or even undesired behaviors due to the potentially abrupt transitions between the torque requests. As the ECMS is a greedy algorithm, i.e., minimizes the cost function at each stage without considering future consequences of the current choice, two consecutive ECMS functions can have completely different local minima, leading to completely different control actions, e.g., engine torque demands. Note that abrupt changes in the control actions will lead to transient processes in the actual plant that are not considered by the model, so the real behavior can deviate from the expected one. This situation usually happens when Equation (26) is non-convex and two local minima can be near in terms of engine speed but far in terms of torque. A conceptual example is provided in Figure 9 where Equation (26) is plotted for different engine torque demands (i.e., control decisions) and engine speed (problem disturbance). It may be observed that the surface has two local minima, and that for close values of engine speeds around 2000 rpm, the minimum jumps abruptly from 40 to 80 Nm. So, eventually, if the vehicle speed varies in a way that the engine speed is around 2000 rpm, the demanded torque will continuously oscillate between 40 and 80 Nm, which, despite being optimal for the model, is probably far from the minimum fuel consumption and acceptable drivability in the actual powertrain.

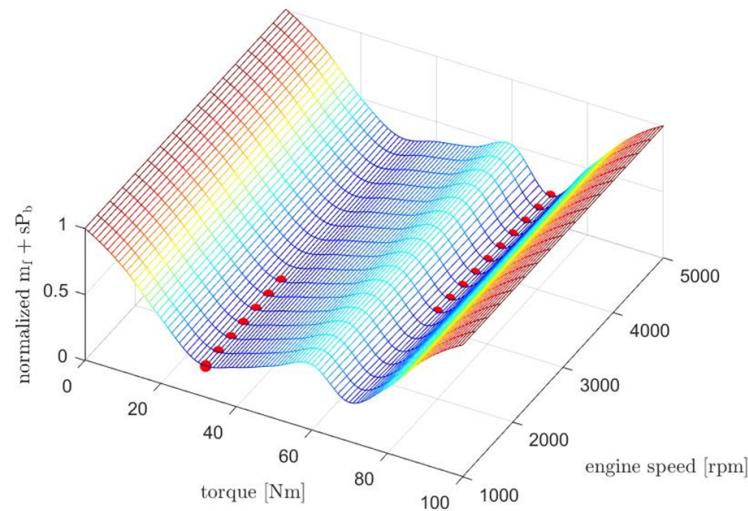


**Figure 9.** Example of non-convexity in Equation (26) leading to strongly different torques minimizing the cost functions at two similar engine speeds.

To cope with this undesired behavior, the following modification of Equation (26) was implemented as observed in Equation (27):

$$u_k^* = \arg \min_u \left\{ P_f(u_k) + sP_b(u_k) + C_{ON}u_{on,k} + C_{du}(u_k - u_{k-1}) + C_\infty((u_k - u_{k-1}) > \overline{du}) + C_\infty((n_k^{eng}ng - n_{k-1}^{eng}ng) > \overline{dn^{eng}}) \right\} \quad (27)$$

where the optimal control at time-step  $k$  ( $u_k^*$ ) is calculated by adjoining the costs for different terms:

- $P_f(u_k) + sP_b(u_k)$  is the direct application of the ECMS, with the particularity that fuel power ( $P_f = \dot{m}_f H_c$ , where  $H_c$  is the fuel heating power) instead of the fuel mass flow is used to allow the  $s$  parameter to be non-dimensional.
- $C_{ON}$  represents the marginal cost of switching on the engine.
- $C_{du}$  is the marginal cost associated with the engine throttle variation.
- $C_\infty$  is an arbitrarily large cost to avoid throttle variations above a certain threshold ( $\overline{du}$ ) or, in the case of the series mode where the engine is decoupled from the wheels, with the engine speed variations above a given limit ( $\overline{dn^{eng}}$ ).

Note that  $C_{ON}$ ,  $C_{du}$ ,  $C_\infty$ ,  $\overline{du}$ , and  $\overline{dn^{eng}}$  are calibration parameters that will depend on the problem addressed.

### 2.3.2. ECMS Modifications to Deal with the Engine's Thermal State

It has been proven in the literature that the engine's thermal state plays a major role in its performance [19]. In this sense, provided that the engine efficiency (and potentially emissions) are strongly affected by the engine's thermal state, the impact of including this variable in the energy management strategy was evaluated.

Considering that the actual engine behaves as the complete model presented in Section 2.2.1, including the lumped-heat transfer model of Equation (4) and its impact on fuel consumption represented by Figure 4. The coolant temperature becomes an additional state of the problem since the past decisions of the maps (engine torque demand, so fuel injection) on future revenues and costs (fuel savings because the engine is warmed up or fuel penalties if the engine is cold due to the lack of operation in previous time-steps). In this sense, the Hamiltonian presented in Equation (20) (or the ECMS cost function in Equation (26)) should be upgraded with an additional state. Accordingly, for this case, Equation (20) was modified into Equation (28):

$$H' = \dot{m}_f + \lambda'_b \dot{E}_b + \lambda'_c \dot{\theta}_c \quad (28)$$

where  $\dot{E}_b$  is the variation of the Energy stored in the battery,  $\dot{\theta}_c$  is the variation of the coolant temperature,  $\dot{m}_f$  is the fuel consumption, and  $\lambda'_b$  and  $\lambda'_c$  are the co-states associated with the battery and coolant. Note that multiplying the fuel consumption by the fuel heating power and the engine temperature by an equivalent thermal capacity of the cooling circuit allows using non-dimensional co-states and power units for  $H$  as presented in Equation (29):

$$H = \dot{E}_f + \lambda_b \dot{E}_b + \lambda_c \dot{E}_c \quad (29)$$

where  $\dot{E}_f$  is the rate of reduction in the energy in the fuel tank,  $\dot{E}_b$  is the rate of reduction in the energy stored in the battery, and  $\dot{E}_c$  is the reduction in the energy stored in the engine's thermal state ( $\dot{E}_c = -C_c \dot{\theta}_c$ ). It can be observed that there is some intuition beyond the application of PMP in Equation (29) since  $H$  represents the rate of reduction in the energy stored (in any form) in the powertrain, and the co-states  $\lambda$  represent the marginal costs of the battery and thermal state. In this sense, minimizing Equation (29) implies that the energy stored in the powertrain is maximized.

Recalling Equation (23) for the co-state associated with the engine's thermal state, the Equation (30) is obtained:

$$\dot{\lambda}_c(t) = - \frac{\partial H}{\partial E_c} = - \frac{\partial H}{\partial (-C_c \theta_c)} = \frac{H_p \partial m_f}{C_c \partial \theta_c} + \lambda_c \frac{C_c \partial \dot{\theta}_c}{C_c \partial \theta_c} \quad (30)$$

where the fuel heating power and the coolant circuit thermal capacity are assumed constants and the battery efficiency is considered independent of the engine coolant temperature. A simple look at Equation (30) shows that  $\lambda_c$  will evolve during the driving cycle since the first term is different from 0 (at least during the warm-up) due to the coolant temperature's effect on engine efficiency and fuel consumption, and the second term will also be different from 0 since the heat transfer in the cooling circuit depends on the coolant temperature (see Equation (4)). In this sense, the ECMS approach considered for the battery (constant  $\lambda_b$ ) cannot be considered for the coolant temperature and  $\lambda_c$  is not constant. Further analysis of Equation (30) shows that the first term on the right side will be non-negative ( $\frac{H_p \partial m_f}{C_c \partial \theta_c} \geq 0$ ) since reducing the coolant temperature involves an increase in the fuel consumption (reduction in efficiency), and the term multiplying the co-state is non-positive ( $\frac{\partial \dot{\theta}_c}{\partial \theta_c}$ ) since increasing the coolant temperature will lead to lower heat coming from the combustion, the process (higher efficiency) and higher heat transfer with the environment. Provided that, in principle, there is no constraint on the terminal state of the coolant temperature, the application of Equation (24) leads to  $\lambda_c(t_f) = 0$ . Hence,  $\lambda_c(t_0)$  should be a value leading to  $\lambda_c(t_f) = 0$  after integration of Equation (30) during the driving cycle. For the

control-oriented model considered in the present project, combining Equation (30) with Equations (2) and (4) with the 3D map presented in Figure 4 leads to Equation (31):

$$\dot{\lambda}_c(t) = \left( -\lambda_c k_{1c} - H_p \frac{\partial h(n, \alpha, \theta_c)}{\partial \theta_c} \left( \frac{1}{C_c} - k_{2c} \lambda_c \right) \right) \quad (31)$$

which can be integrated to compute the evolution of  $\lambda_c$ . Therefore, considering the engine’s thermal state leads to the initial value problem, with two initial values to determine:  $s$  (provided constant  $\lambda_b$ ) and  $\lambda_c$ . Both values can be obtained by a shooting method until the desired final SOC and  $\lambda_c(t_f) = 0$  are reached. In practical cases, due to the complexity of numerically integrating Equation (30), it is difficult to reach  $\lambda_c(t_f) = 0$  and the value of  $\lambda_c(t_0)$  is chosen in a way that minimizes fuel consumption. A similar approach to that followed in this model can be found in [16].

### 2.3.3. ECMS Modifications to Account for Different Powertrain Modes

The ECMS is prepared to work with series and parallel architectures with different gear ratios. To this aim, several optimizations are running at the same time that provide the optimal control outputs (demanded torques for the ICE and electric machines) and the associated cost of every mode. Then in a second optimization stage, the best option amongst the available modes is selected. Figure 10 shows the general scheme as follows:

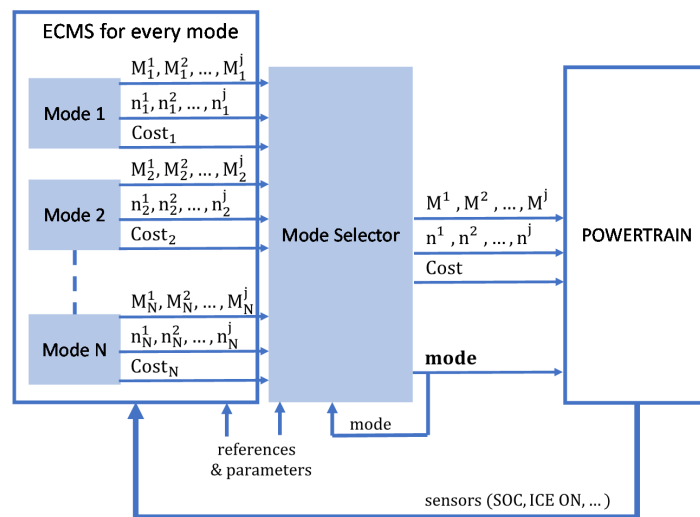


**Figure 10.** Scheme of the extension of the ECMS to integrate several ( $N$ ) modes and the corresponding torque and speed demands of the  $j$  engines and electric machines.

- (a) The ECMS is applied independently for the  $N$  modes available in the powertrain. In this sense, for every powertrain mode  $i$ , the optimal speed and torque for any of the  $j$  engines and motors ( $n_i^j, M_i^j$ ) with its corresponding minimum cost ( $Cost_i$ ) is calculated.
- (b) The previous information arrives at the mode selector, where the option with minimum cost is chosen. Directly comparing the cost of the different modes might result in a highly oscillating control policy, especially since the model barely addresses the system dynamics, which will not produce desirable results when applying the control to the actual powertrain. Every time a switch between modes is carried out, the powertrain experiences a transient that the model is not able to consider. To cope with this issue, the following optimization is proposed (Equation (32)):

$$u_{mode,k}^* = \arg \min_{i \in [1,N]} \sum_{k-\Delta k}^k \{ Cost_{i,k} + C_{dmode}(i - u_{mode,k-1}^*) + C_{mode,i} \} \quad (32)$$

where  $u_{mode,k}^*$  is the optimal mode to be applied at time-step  $k$ ,  $Cost_{i,k}$  represents the cost of mode  $i$  at time-step  $k$ ,  $C_{dmode}$  is the cost of modifying the mode (so is 0 if the same mode in the previous time-step is employed) and  $C_{mode,i}$  is an artificial cost to avoid the use of a particular mode (e.g., to ban the use of the series mode in a vehicle that has parallel architecture exclusively). Finally,  $\Delta k$  is a parameter to consider the mode minimizing the cost during a given time window instead of the instantaneous one. Note that  $C_{dmode}$ ,  $C_{mode,i}$ , and  $\Delta k$  are parameters to calibrate.

### 3. Results

In order to assess the impact of taking into account the engine's thermal state (TS) in the control strategy, the worldwide harmonized light vehicle test cycle (WLTC) and RDE cycles were selected for the simulation and experiment. The velocity profiles of both cycles were used as inputs (i.e., vehicle speed demand) for the integrated model. Simulation results showed the optimum power split computed by the EMS of the integrated model. Afterward, the speed and torque profiles of the internal combustion engine were launched on the test bench. For all of the cases, the energy management strategy consisted of the battery charge sustain (i.e., both initial and end battery capacity at 50%). Hence, the lower the engine fuel consumption at the end of the cycle, the higher the operation efficiency of the system. It is important to state that additional requirements were added to the control strategy in the model due to the test bench requirements. The ICE switching period was set to 16 s since a higher ICE switching frequency was not possible to follow in the test bench. Furthermore, the tuning of the parameter representing the cost of turning on the engine was necessary to equal the brake energy of both control strategies since only the ICE was experimentally tested.

#### 3.1. WLTC Cycle

In Figure 11, it can be seen that in both control strategies, taking into account the engine's thermal state (TS on) and without it (TS off), the vehicle speed demand is fulfilled. Although the selections of the power split distributions in both control strategies were very different, the final battery SOC was practically the same, complying with the simulation requirements. On the one hand, when the engine's thermal state control strategy is activated, almost half of the WLTC cycle is run in an electric mode and the battery is discharged until 45% at 800 s. At this moment, the engine is turned on for the rest of the cycle. The EMS decides that using the engine in the most power-demanding part of the cycle will reduce the energy consumption. On the other hand, in the case of 'TS off', the engine is used from the beginning and is turned off when using it costs more than using the energy stored in the battery. It can be seen that the battery starts discharging during the last half of the cycle when more overall power is demanded.

In Figure 12, the comparison between the experimental and simulation results is presented for the WLTC cycle. The evolution of the engine torque, accumulated fuel consumption, and coolant temperature are shown for both control strategies. It can be seen that there is good agreement between both experimental and simulation torques. Some braking discrepancies were observed for the 'TS off' the case; however, the experiment's accurately replicated the torque profile provided by the simulation. The trend of the accumulated fuel consumption was completely captured in the experimental measurements. Additionally, in both the simulation and experiments, 'TS on' presents a lower fuel consumption, as can be appreciated in the (c) and (d) plots of Figure 12. The fuel savings with the 'TS on' strategy were around 3.6% and 4.1% for the simulation and experiment, respectively. This difference could be explained by the fact that the model underestimates the fuel consumption during the turning on of the engine, given the fact that for both control strategies, the model slightly underestimates the experimental fuel consumption since the model does not capture the surplus fuel injected during the engine start. The discrepancy in the torque profile could also contribute to the discrepancy. Overall, taking into account the engine's thermal state (TS on) has shown great fuel-saving gains since operating the ICE at higher



temperatures significantly reduces power friction and increases the combustion efficiency. Plots (e) and (f) of Figure 12 show that with 'TS off', the engine runs to the time out of its optimum temperature range (between 0 and 1000 s). Furthermore, the warm-up (engine coolant temperature higher than 85 °C) time is higher. However, 'TS on' only turns on the engine when it really needs it and the warming-up process is much faster since it runs at higher demanding conditions. Note that the slope of the coolant temperature evolution is higher than the two ICE warming phases present in the 'TS off' case.

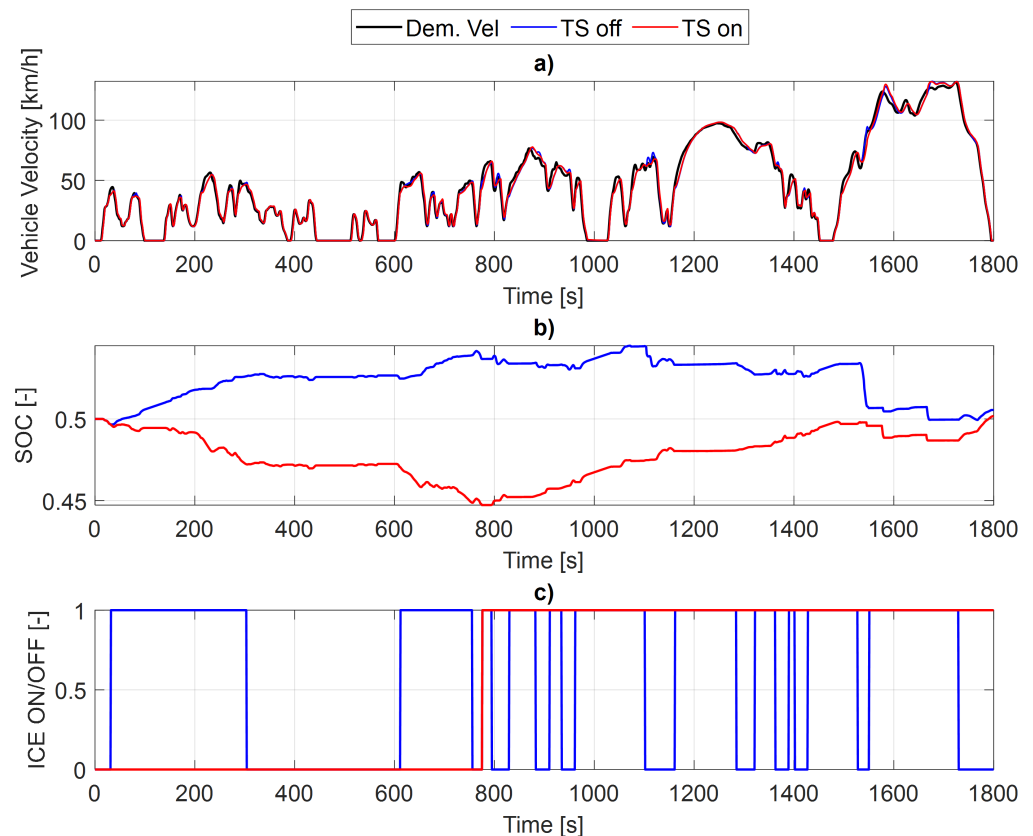


**Figure 11.** Simulation results for both control strategies during the WLTC cycle. (a) Vehicle velocity. (b) State of Charge of the Battery (SOC). (c) ICE switch.

### 3.2. RDE Cycle

In Figure 13, the results of both control strategies for the simulation of the RDE cycle are presented. Similarly to the previous cycle, the vehicle velocity demand was fulfilled by the energy management system in both control strategies. The SOC evolution shows that until almost 1000 s, both power split distributions were the same. Then, the control strategy 'TS off' turns on the engine and starts charging the battery while 'TS on' still delays the ICE starting for more demanding conditions. Furthermore, the ICE switching number is higher in the 'TS off' than in the 'TS on' case, as it happens in the previous cycle. It seems that taking into account the thermal state of the engine reduces the switching frequency of the engine. It is reasonable that the control strategy searches for the optimum time for turning the engine while reducing the number of stops and, hence, avoiding ICE cooling and further operations at low temperatures.

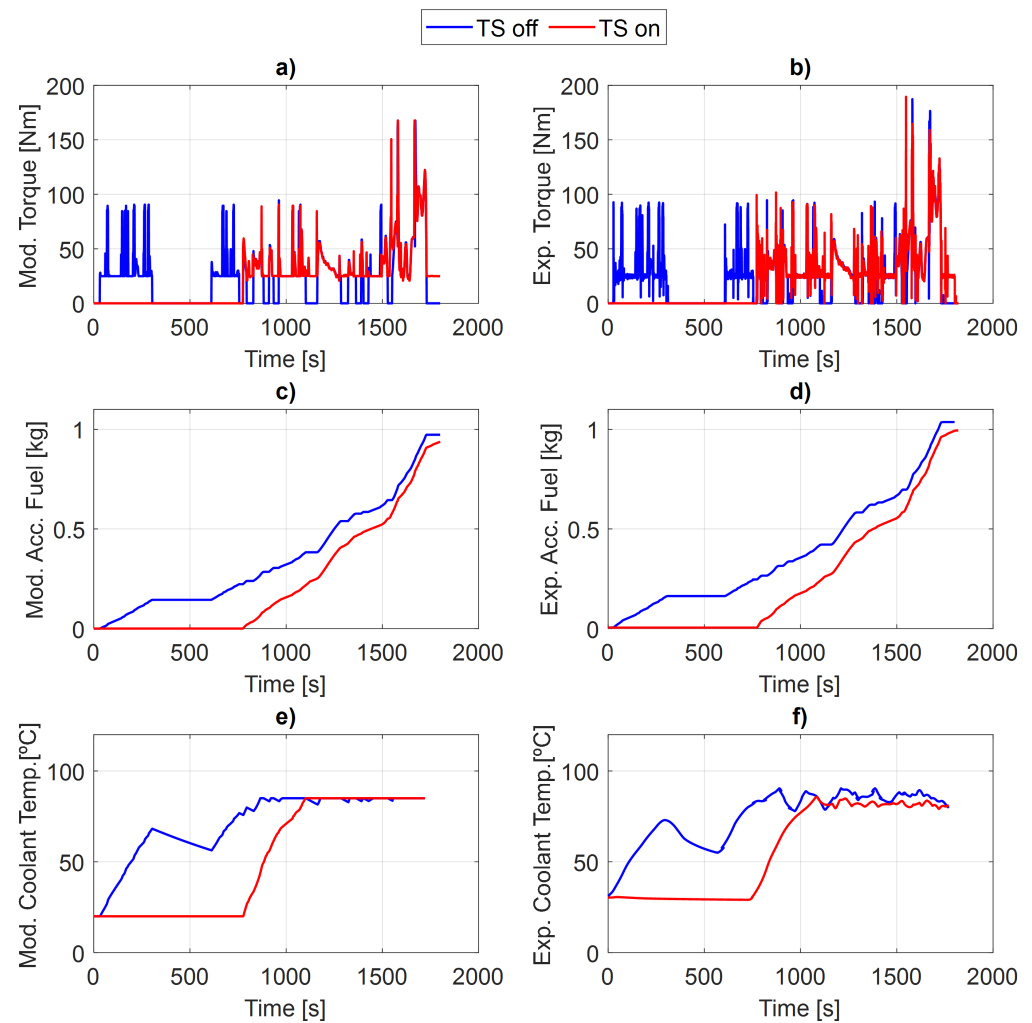


**Figure 12.** Comparison between both strategies for ICE simulation results (left plots) and experimental measurements (right plots) during the WLTC cycle. (a) Model torque. (b) Experimental torque. (c) Model fuel consumption. (d) Experimental fuel consumption. (e) Model coolant temperature. (f) Experimental coolant temperature.

A significant agreement between the simulation results and experimental measurements can be observed in Figure 14. The coolant temperature error after the thermostat opens (warming up of the engine) is higher than during the rest of the cycle because the lumped thermal model of the engine does not include the real behavior of the thermostat. However, this is not relevant to the study since most of the impact of the strategy is obtained during the engine warming up. Additionally, the trends are captured. The evolution of the accumulated fuel consumption shows that the ‘TS on’ control strategy is more efficient. Fuel savings were around 4% and 3% for the simulation and experiments, respectively. These gains are very similar to the ones obtained for the WLTC cycle.

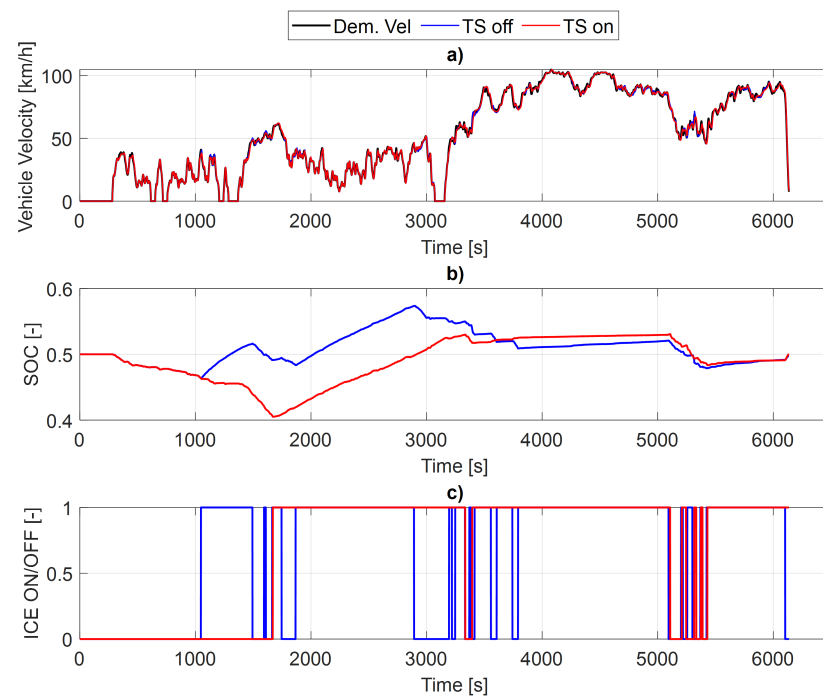


**Figure 13.** Simulation results for both control strategies during the RDE cycle. (a) Vehicle velocity. (b) State of charge of the battery (SOC). (c) ICE switch.

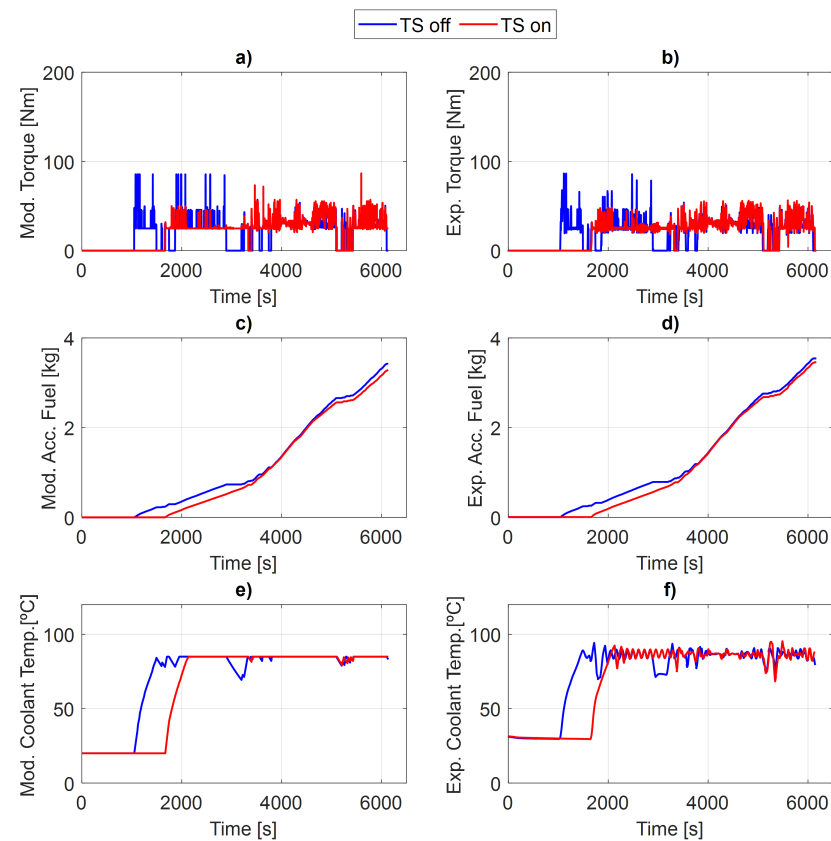


**Figure 14.** Comparison between both strategies for ICE simulation results (left plots) and experimental measurements (right plots) during the RDE cycle. (a) Model torque. (b) Experimental torque. (c) Model fuel consumption. (d) Experimental fuel consumption. (e) Model coolant temperature. (f) Experimental coolant temperature.

#### 4. Conclusions

The main conclusions of this work can be summarized as follows:

- An integrated virtual model for the energy management of xEVs was developed and the study of a hybrid electric vehicle was carried out with this tool. The programmed control strategy is based on the ECMS, while additional terms to compensate for dynamic issues, to consider other potential powertrain architectures and states, such as the engine's thermal state, have been added. The energy management strategy is able to consider the engine's thermal state in the control algorithm, which is a novelty with respect to the state-of-the-art ECMS. In order to implement this, an extensive experimental campaign was performed at different engine coolant temperatures in order to implement a temperature-dependent 3D map.
- Simulation results show that, taking into account the thermal state (TS on) of the engine reduces the fuel consumption when compared to the base case. Experimental measurements confirmed those gains in both cycles. The 4.1% and 3% accumulated fuel reductions were obtained for the WLTC and RDE cycles, respectively. This is because when the control strategy considered the thermal state of the engine, the engine was turned on only when its warming-up time was going to be the fastest and the engine operated at maximum times at higher temperatures. This contributes to decreasing power losses and increasing ICE fuel consumption.

**Author Contributions:** Conceptualization, A.D.; Methodology, A.B., P.O. and B.P.; Software, B.P.; Writing—original draft, A.D.; Writing—review & editing, P.O. and B.P.; Supervision, A.B. All authors have read and agreed to the published version of the manuscript.

**Funding:** The authors sincerely acknowledge the founding support provided by Conselleria de Innovación, Universidades, Ciencia y Sociedad Digital in the framework of the Ayuda Predoctoral GVA. (ACIF/2020/234).

**Institutional Review Board Statement:** Not applicable.

**Informed Consent Statement:** Not applicable.

**Data Availability Statement:** Not applicable.

**Acknowledgments:** The authors sincerely acknowledge the support provided by Renault S.A.S. (RSA).

**Conflicts of Interest:** The authors declare no conflict of interest.

#### Abbreviations

The following abbreviations are used in this manuscript:

EV	electric vehicles
EMS	energy management system
DP	dynamic programming
PMP	Pontryagin's minimum principle
ECMS	equivalent consumption management strategy
MPC	model predictive control
BSFC	brake specific fuel consumption
ICE	internal combustion engine
ICEV	internal combustion engine vehicle
PHEVS	plug-in hybrid electric vehicles
SOC	state of charge
PID	proportional–integral–derivative controller
FMU	functional mock-up unit
RDE	real driving emission
WLTC	worldwide harmonized light vehicle test cycle
HSG	high-voltage starter generator
EM	electric motor

## References

1. IEA. *Global EV Data Explorer*; IEA: Paris, France, 2021.
2. Tappeta, V.S.R.; Appasani, B.; Patnaik, S.; Ustun, T.S. A Review on Emerging Communication and Computational Technologies for Increased Use of Plug-In Electric Vehicles. *Energies* **2022**, *15*, 6580. [\[CrossRef\]](#)
3. Tsiropoulos, I.; Siskos, P.; Capros, P. The cost of recharging infrastructure for electric vehicles in the EU in a climate neutrality context: Factors influencing investments in 2030 and 2050. *Appl. Energy* **2022**, *322*, 119446. [\[CrossRef\]](#)
4. Karoń, G. Safe and Effective Smart Urban Transportation—Energy Flow in Electric (EV) and Hybrid Electric Vehicles (HEV). *Energies* **2022**, *15*, 6548. [\[CrossRef\]](#)
5. Polverino, P.; Arsie, I.; Pianese, C. Optimal Energy Management for Hybrid Electric Vehicles Based on Dynamic Programming and Receding Horizon. *Energies* **2021**, *14*, 3502. [\[CrossRef\]](#)
6. Xue, Q.; Zhang, X.; Teng, T.; Zhang, J.; Feng, Z.; Lv, Q. A Comprehensive Review on Classification, Energy Management Strategy, and Control Algorithm for Hybrid Electric Vehicles. *Energies* **2020**, *13*, 5355. [\[CrossRef\]](#)
7. Onori, S.; Serrao, L.; Rizzoni, G. *Hybrid Electric Vehicles: Energy Management Strategies*; Springer: Berlin/Heidelberg, Germany, 2016.
8. Sundström, O.; Ambühl, D.; Guzzella, L. On Implementation of Dynamic Programming for Optimal Control Problems with Final State Constraints. *Oil Gas Sci. Technol. Rev. IFP* **2010**, *65*, 91–102. [\[CrossRef\]](#)
9. Ozatay, E.; Onori, S.; Wollaeger, J.; Ozguner, U.; Rizzoni, G.; Filev, D.; Michelini, J.; Di Cairano, S. Cloud-Based Velocity Profile Optimization for Everyday Driving: A Dynamic-Programming-Based Solution. *IEEE Trans. Intell. Transp. Syst.* **2014**, *15*, 2491–2505. [\[CrossRef\]](#)
10. Martinez, C.M.; Hu, X.; Cao, D.; Velenis, E.; Gao, B.; Wellers, M. Energy Management in Plug-in Hybrid Electric Vehicles: Recent Progress and a Connected Vehicles Perspective. *IEEE Trans. Veh. Technol.* **2017**, *66*, 4534–4549. [\[CrossRef\]](#)
11. Kessels, J.; Koot, M.; van den Bosch, P.; Kok, D. Online Energy Management for Hybrid Electric Vehicles. *IEEE Trans. Veh. Technol.* **2008**, *57*, 3428–3440. [\[CrossRef\]](#)
12. Hwang, H.Y. Developing Equivalent Consumption Minimization Strategy for Advanced Hybrid System-II Electric Vehicles. *Energies* **2020**, *13*, 2033. [\[CrossRef\]](#)
13. Zhang, B.; Zhang, J.; Xu, F.; Shen, T. Optimal control of power-split hybrid electric powertrains with minimization of energy consumption. *Appl. Energy* **2020**, *266*, 114873. [\[CrossRef\]](#)
14. Van Berkel, K.; Klemm, W.; Hofman, T.; Vroemen, B.; Steinbuch, M. Optimal Energy Management for a Mechanical-Hybrid Vehicle with Cold Start Conditions. In Proceedings of the 2013 European Control Conference (ECC), Zürich, Switzerland, 17–19 July 2013.
15. Chu, H.; Shi, H.; Jiang, Y.; Shen, T. Modeling of engine thermal dynamics and its application in energy management of HEVs considering engine warming-up. *Int. J. Engine Res.* **2021**, 146808742110445. [\[CrossRef\]](#)
16. Lescot, J.; Sciarretta, A.; Chamaillard, Y.; Charlet, A. On the integration of optimal energy management and thermal management of hybrid electric vehicles. In Proceedings of the 2010 IEEE Vehicle Power and Propulsion Conference, Lille, France, 1–3 September 2010.
17. Luján, J.M.; Guardiola, C.; Pla, B.; Pandey, V. Impact of driving dynamics in RDE test on NOx emissions dispersion. *Proc. Inst. Mech. Eng. Part D J. Automob. Eng.* **2020**, *234*, 1770–1778. [\[CrossRef\]](#)
18. Broatch, A.; Olmeda, P.; Margot, X.; Agizza, L. A generalized methodology for lithium-ion cells characterization and lumped electro-thermal modelling. *Appl. Therm. Eng.* **2022**, *217*, 119174. [\[CrossRef\]](#)
19. Broatch, A.; Olmeda, P.; Martín, J.; Dreif, A. Improvement in engine thermal management by changing coolant and oil mass. *Appl. Therm. Eng.* **2022**, *212*, 118513. [\[CrossRef\]](#)

**Disclaimer/Publisher’s Note:** The statements, opinions and data contained in all publications are solely those of the individual author(s) and contributor(s) and not of MDPI and/or the editor(s). MDPI and/or the editor(s) disclaim responsibility for any injury to people or property resulting from any ideas, methods, instructions or products referred to in the content.